X-661-75-114
PREPRINT

TEMPORAL X-RAY ASTRONOMY WITH A PINHOLE CAMERA

STEPHEN S. HOLT

MAY 1975

GODDARD SPACE FLIGHT CENTER
GREENBELT, MARYLAND

TEMPORAL X-RAY ASTRONOMY WITH A PINHOLE CAMERA

Stephen S. Holt

Invited paper A.2.10 presented at the COSPAR Symposium on Fast Transients in X- and Gamma-Rays, Varna, Bulgaria.

May 1975

Abstract

The first preliminary results from the Ariel-5 All-Sky X-Ray Monitor are presented, along with sufficient experiment details to define the experiment sensitivity. Periodic modulation of the X-ray emission is investigated from three sources with which specific periods have been associated, with the results that the 4.8 hour variation from Cyg X-3 is confirmed, a long-term average 5.6 day variation from Cyg X-1 is discovered, and no detectable 0.787 day modulation of Sco X-1 is observed. Consistency of the long-term Sco X-1 emission with a "shot-noise" model is discussed, wherein the source behavior is shown to be interpretable as ~ 100 "flares" per day, each with a duration of several hours. A sudden increase in the Cyg X-1 intensity by almost a factor of three on 22 April 1975 is reported, after 5 months of relative source constancy. The light curve of a bright nova-like transient source in Triangulum is presented, and compared with previously observed transient sources. Preliminary evidence for the existence of X-ray "bursts" with duration < 1 hour is offered, with the caveat that there is not yet any supporting evidence to guarantee that the effect is truly astronomical.

The All-Sky Monitor on-board Ariel-5 is the first true imaging X-ray astronomy experiment to be flown on a scientific satellite. It is also, perhaps, the smallest X-ray astronomy experiment which will ever be flown, with an effective area of only 1 cm^2 and a total experiment weight of about 2kg. Its purpose is to monitor the entire sky continuously for transient X-ray phenomena and, at the same time, to monitor all the strong sources in the sky for long-term temporal effects.

The basic approach to the All-Sky Monitor is the utilization of X-ray pinhole cameras to image the sky. It is important to point out that these need be <u>true</u> imaging pinholes (i.e. not a multi-pinhole Dicke camera). This is because most of the counts detected are from a large number of <u>variable</u> sources, so that there must be a unit transformation from the detector to the sky in order to be sure that intensity variations are uniquely assigned.

The optimization of the detector geometry begins with the assumption of an aperture size (area a^2), and a detector element (area b^2) a height h below the aperture. The internal background in the detector element is

$$I = I_o b^2,$$

and the "background" from the diffuse X-ray sky imaged through the aperture is

$$B = B_o \frac{a^2 b^2}{h^2}$$

The source exposure in the element is

$$S = S_o a^2 \qquad a < b$$

$$= S_o b^2 \qquad a > b$$

Using the traditional definitions of signal-to-noise, we have (for $B \gg I$)

$$\frac{S}{\sqrt{B}} = \frac{S_o}{\sqrt{B_o}} \; h \; \frac{a}{b} \qquad a < b$$

$$= \frac{S_o}{\sqrt{B_o}} \; h \; \frac{b}{a} \qquad a > b,$$

i.e the sensitivity is best for $a = b$, and is (in fact) independent of a. This means that the formal sensitivity (for a detector of low internal background) is dependent only on the distance from aperture to detector, and an accumulation time long enough to assure that the exposure is not quantum limited. Even in the other background limit ($I \gg B$),

$$\frac{S}{\sqrt{I}} = \frac{S_o}{\sqrt{I_o}} \; \frac{a^2}{b} \qquad a < b$$

$$= \frac{S_o}{\sqrt{I_o}} \; b \qquad a > b,$$

so that $a = b$ again for optimum signal-to-noise. Therefore, an optimized pinhole camera should have $a \approx b$ whatever the primary source of background. The remainder of the optimization procedure is purely pragmatic. Given the operational constraints (in this case, the size, weight and data allowances provided by Ariel-5), the iteration to the final geometry is fairly straightforward. The available volume fixes the pinhole size at ~ 1 cm^2, but the weight and viewing obstructions

make it impossible to consider viewing the entire sky all the time. Since the satellite rotates, however, the whole sky can be monitored (at least once per rotation) if the camera has a fan beam response. This geometry is displayed in Figure 1, where two position-sensitive proportional counters are used to record the photons imaged through the pinholes. The walls of the box (including a dividing wall between the two cameras) are made of honeycomb to keep the weight low, with ~ .1mm of titanium for X-ray opacity backed by aluminum (to absorb the K-fluorescence of the titanium). This provides a very low weight "light-tight" (for X-rays in the energy range of the experiment) pinhole camera. Its configuration on the satellite is such that the fan beam response is completely unobscured.

The position-sensitive proportional counters use simple charge division between two charge-sensitive preamplifiers at either end of a carbon-loaded highly resistive quartz anode to define the position of ionizing events. The anode is 25 μm in diameter, with a resistance per unit length of ~ 1 Megohm cm^{-1}. In order to make the position determination insensitive to the total energy deposition, standard ramp rundown analyzing techniques are used to define the position via the ratio of the charge collected at one end of the anode to the total of the charge collected at both ends. This is not the most precise way to perform this location (as timing techniques can do better), but simple charge division can give a position resolution of $\leq$ 1 mm over the active length of ~ 30 cm, and this is an order of magnitude better than the experiment requires.

The detector internal background is kept low by the combination of three effects. One is the relatively clean near-equatorial orbit (near-circular, with altitude ~ 500 km). The other two are designed right into the detectors. Position sensitivity allows the rejection of events at the ends of the counter trivially (i.e. by not including the outermost ~ 1 cm of anode at each end in analysis), and there is active anti-coincidence completely surrounding the position-sensitive volume on all sides except the entrance port, as shown in Figure 2. The relatively thick Be window (5 mils) sacrifices some efficiency in order to guarantee a well-defined acceptance window for X-rays. As the data limitation does not allow the luxury of more than a single energy window, it is important that the window response remain stable. The electronic thresholds are set at 2.5 keV and 7.5 keV (energy equivalent at nominal gain), and Figure 3 indicates that the gain can change by as much as a factor of two before any noticeable degradation in response can be observed. There are four high voltage positions built into the experiment should the gain change due to gas leakage (determinable from the measured flux from the Crab Nebula and the average internal background), but thus far the gain shift has remained stable. The average background in the detectors in orbit is approximately 2×10^{-3} $cm^{-2} sec^{-1} keV^{-1}$.

Ariel-5 has no tape recorder, operates for only the 2/3 of each ~90-minute orbit which is sunlit, and has no capability for transmitting experiment data to the ground in real-time. All the experiment data is gathered into a core-store memory and telemetered to the ground once per orbit. The allocation of the core-store memory to the All-Sky Monitor

is such that 512 elements can be utilized for separate one-orbit accumulations. If all of these are used for resolution elements on the sky, these cannot average much less than ~ 10° on a side, so that it is fruitless to consider attempting to take advantage of the inherent energy resolution of the proportional counters. The quartz anodes are quite uniform, and the resolution obtained in the laboratory with flight counters was 16% FWHM for Fe^{55} at 5.9 keV.

The final tactical decision was to divide the 512 elements into 16 spacecraft latitude elements (8 per proportional counter) and 32 longitude elements corresponding to phases of the spacecraft 10 rpm rotation relative to the sun. This scheme is illustrated in Figure 4, where the 512 elements are shown in spacecraft coordinates. The elements are arranged in an electronically convenient way to be generally consistent with a uniform source sensitivity (i.e. elements nearer the equator, where the effective on-time is shortest, have smaller latitude extensions to keep the background lower). Dead bands were purposely introduced near the spacecraft poles and spacecraft equator, because the pinhole apertures were least efficient there, and other Ariel-5 instruments view along the spin axis and in the equatorial band with higher sensitivity than the All-Sky Monitor. If the sun is not in the equatorial band of the spacecraft, its high intensity relative to celestial sources saturates the experiment response in its vicinity, but the solar image is always well localized and does not introduce appreciable background into the remainder of the experiment resolution elements. The image of the sun in Figure 4 is typical of the experiment response to point

sources ($\sim 4° \times 4°$) in this mode of operation, so that sources may contribute to as many as 4 elements, but contribute to only 1 or 2 more often than not.

The capacity of each resolution element readout is $2^8-1 = 255$ counts, after which it recycles. Since Sco X-1 will usually recycle its element, we have an overflow capability which sums the detected counts from each counter at a given spacecraft longitude (i.e. the sum of eight elements) into one of 64 one-orbit accumulations with a capacity of $2^{16}-1$. This summing is performed at the front end (i.e. each ionizing event is counted into both accumulators separately at detection), so that the data may be easily checked for telemetry errors if the sums do not agree. Thus far, there has been only one seemingly good orbit for which the sums did not agree, with a difference of a single counted photon.

There is a second mode of operation of the experiment which should be mentioned for the sake of completeness. As the data restrictions do not allow the a = b optimization condition to be realized, and since the location of a transient effect to ~10° is worse than the inherent resolution of the pinhole, it is possible to command the experiment to a mode in which all 512 elements are confined to 1/16 of the sky. The resolution in both latitude and longitude are each bettered by a factor of four, resulting in a typical resolution element of $\sim 2° \times 2°$ and a nearer realization to the a = b optimization condition. This mode is used only for better localization of transient phenomena, however, as it violates the prime requirement of continuous full-sky coverage.

Figure 5 is a reproduction of part of the raw data from a representative orbit which illustrates the quantum limitation of the experiment. Spacecraft latitude and earth occultation conditions affect the number of counts recorded from each source each orbit, as well as the background in the elements to which the source contributes. This orbit was chosen as "typical" solely because the five sources indicated happened to be confined almost entirely to single resolution elements (a relatively atypical phenomenon, in fact), but the important information here is that Sco X-1 can generally be expected to provide several hundred counts (in the illustrated orbit: 31 counts from the raw 512-element data plus 256 counts corresponding to the overflow, as the two accumulators differed by precisely 256), while other sources can be expected to contribute considerably less. This is the fundamental limitation of an aperture of 1 cm^2 with a duty cycle of ~1% for a given source, so that low counter background and gain stability are absolutely essential to a meaningful analysis of these data.

An excellent test of the true experiment sensitivity is afforded by Cyg X-3, which has a well-known 4.8 hour periodicity. As the angular separation between Cyg X-3 and Cyg X-1 is comparable with the separation between adjacent resolution elements, and since 4.8 hours is only slightly more than three orbits, the ability to detect this effect would be a welcome assurance that systematic effects do not dominate the experiment response. This assurance is demonstrated in Figure 6, where single-orbit data from both Cyg X-1 and Cyg X-3 have been folded at 4.8 hours. In order to preserve the statistical independence of each bin,

the deduced magnitude from each orbit contributes to only a single bin corresponding to the orbit mid-time, even though the total accumulation time of each orbit may stretch across as many as seven bins. The relatively smooth sinusoid obtained for Cyg X-3 therefore, is not an artifact resulting from the use of the same data in more than one bin. Both the amplitude and phase of the modulation are consistent with those reported previously by Parsignault et al. (1972), Sanford and Hawkins (1972), and Canizares et al. (1973).

There still remain systematic effects (mostly associated with pointing errors) which have not been entirely removed in the data analysis, and which compromise the search of source data for periodicity. For this reason, only tests at periods which have been specified from other evidence will be presented here. If source data is folded at a prescribed period (and another source used as a control), we can be reasonably certain that any modulation detected does not arise from systematic errors.

We have detected a 5.6 day modulation of the Cyg X-1 emission, which is illustrated in Figure 7. The first trace is a fold of several months of Cyg X-1 data at 5.4 days, which gives no indication of modulation at this trial period. The fourth trace is similarly featureless Crab Nebula data taken over the same time interval folded at 5.6 days. Cyg X-1 at 5.6 days, however, gives an unacceptable value of χ^2 (with the hypothesis of no modulation). The value of χ^2 is not so unacceptable as to provide convincing proof of modulation without supporting evidence, as 5.3 days (in the third trace) happens to give a similarly unacceptable

value. The significant difference between the two is that the 5.3 day χ^2 can be decreased to the acceptable level by binning differently, as the large contribution to this χ^2 comes from positive and negative decrements in adjacent bins; the 5.6 day effect is stationary if the binning phase is changed.

A second reason for believing that true modulation is observed is the fact that the minimum is consistent with phase = 0, or superior conjunction, for the binary system. Third, the data displayed in Figure 7 broken into smaller total accumulation times (as well as data obtained subsequently) usually (but not always) demonstrate a relative minimum near $\phi = 0$, although it is not always statistically significant.

The magnitude of the modulation in Figure 7 is quite important, as it amounts to an average decrement of more than 1% of the total light curve averaged over several months. As the absorption dips measured by Copernicus (Mason, et al. 1974) and OSO (Li and Clark, 1974) have typical times of $\leq$ 1 hour, it is difficult to see how such dips alone can account for the modulation, as a one hour dip corresponding to even as much as 10^{24} H-atoms cm^{-2} in the line of sight <u>every</u> cycle would fall short by a factor of two in producing the observed effect. Dips are not present each cycle (in fact, they appear to occur less than half the time, with a phase which may be almost 10% of the light curve away from $\phi = 0$). Our statistics do not allow the unambiguous measurement of individual dips, so the data which go into Figure 7 are averaged over several orbits when the pointing direction is stable (but never more than half a day). The fold for single orbit data does not differ substantially,

however, so that it would appear that sharp $\leq$ 1 hour dips alone cannot account for the modulation.

Since such modulation was not observed in 40 continuous days of UHURU observation (Tananbaum et al., 1972), and since the effect in the present data is not always detectable, it would appear that this modulation (like the absorption dip phenomenon) is not reproducible from cycle to cycle. A possible explanation of the modulation may be that the stream of cold matter between the two components of the binary system responsible for the absorption dips (Hutchings, et al. 1973) has sufficient extent to shadow the X-ray source at a relatively low level of absorption for times of the order of a day, in addition to a sharp minimum if and when the higher density core of the stream intercepts the line of sight to the X-ray source. This would produce a more consistent modulation of the emission at 5.6 days near $\phi = 0$ than the narrow dips alone, but one which could also vary considerably in time. An average line-of-sight column density of $\geq 10^{22}$ H-atoms cm^{-2} for $\sim$ 1 day would then be all that would be required to produce the observed modulation.

It is worth noting that Cyg X-1 has been remarkably constant during the first few months of the satellite operation. Although renowned for its sporadic behavior, it exhibited less variation than the other two sources in Cygnus until 22 April 1975. At that time, as shown in Figure 8a, it almost trebled its intensity for about a week, at which time it passed out of the field of view of the experiment. No other variations

of this magnitude and duration from the source have been observed since the onset of data accumulation in November of 1974. The intensity variations in the daily averages of Figure 8a appear to be real, and ~ half-day averages and errors for the rising portion of the source are shown in Figure 8b. The statistical errors do not allow finer resolution with this experiment.

Another source for which a binary period has been assigned from its optical counterpart is Sco X-1 (Gottlieb, Wright and Liller, 1975). In Figure 9, data from ~ 100 days is folded modulo 0.787313d, with no apparent modulation of the X-ray emission. The value of χ^2 is clearly unacceptable, but it is similarly unacceptable for any other folding period. This is because Sco X-1 exhibits substantial non-periodic variation, and a few months is not sufficiently long a time for these non-periodic variations to average out. For this reason, we cannot place an upper limit on any 0.787313d variation from Sco X-1 in the traditional way. From test simulations, however, a regular sinusoidal variation with amplitude $\geq$ 10% of the average value could have been unambiguously detected in the presence of non-periodic variations.

The variations from Sco X-1 are extremely large, with a maximum intensity about a factor of three higher than minimum. Figure 10 is an orbit-by-orbit history of Sco X-1 during a particularly disturbed period in January of 1975, where orbits just a few hours apart have average intensities which differ by almost a factor of two. It is important to note, however, that the disturbances are typically several hours in extent, as the orbit-to-orbit variations appear to be

correlated on time scales of the order of a large fraction of a day. This observation is borne out by Figure 11, which compares the intensity from Sco X-1 with the mean intensity measured over three months of 16.5 $cm^{-2}sec^{-1}$, as a function of accumulation time. The difference between the local intensity and the average, divided by the estimated statistical error in the local intensity, is just the square root of the ratio of actual to expected variances if the measured Sco X-1 intensity is a Poisson variable. The expectation value for such a ratio would then be unity independent of accumulation time and the plotted "expectation" in Figure 11 is the mean of all such terms calculated for a given timescale.

The single-orbit expectation value is in excess of 10, but it steadily increases to an asymptotic value ~50 for accumulation times in excess of ~ 1 day. The simplest interpretation of this behavior is in terms of a "shot-noise" source model, as has been discussed for Cygnus X-1 on much shorter timescales (Boldt et al. 1975). If we assume that all of the Sco X-1 intensity can be presumed to arise from "flares", the intensity and duration of a typical flare can be estimated from the fact that flare statistics dominate counting statistics. A consistent set of parameters which can simulate Figures 10 and 11 is a Sco X-1 emission dominated by ~100 "flares" per day, each having a duration of no more than ~ 1/2 day.

Several very strong transient sources have been observed during the past few months - more, in fact, than would have been expected from previous work. At least three have been discovered with an apparent

magnitude at maximum rivalling that of the Crab Nebula. All three have been observed by this experiment, with various degrees of confusion problems with other sources. One, at galactic center, was completely confused - we could not tell whether a new source was present, or whether the emission arose from one of the other strong sources near galactic center. Even knowing its position, we could not unambiguously assign its intensity.

The situation was much better for the source in Triangulum first reported by Pounds (1974). Although close to Cir X-1, the absence of the latter source during late 1974 and early 1975 has made it possible to construct an unambiguous light curve for this nova-type transient source, as shown in Figure 12.

In common with other nova-type transient sources, this one exhibits a two-component decay. After a maximum apparent magnitude close to that of the Crab Nebula, it levels off for about two weeks before decaying with an e-folding time of ~ two months. After the discovery of this source, we searched earlier data for its presence. If Cir X-1 is truly ≤ 50 UHURU counts during this time, so that confusion is no problem, we find an extended on-state for the nova source at ~ 10% of its maximum level. This is the first instance in which such a source is found at a prolonged on-state prior to outburst, and may rule out some models which require a critical instability to flash the source. A comparison of its history with other nova sources is given in Figure 13, where the synthetic light curve of Amnuel, et al. (1974) has been used to normalize the time scales (i.e. phase = 0 is maximum intensity, phase = 1

is one-tenth maximum intensity).

Another such source has just been found near the Crab Nebula, and some empirical facts about the nature of such sources is now beginning to emerge. Silk (197) demonstrated quite elegantly that the transient sources could not be extragalactic, and concluded that they were probably population I objects which occurred at a rate of ~ 5 year^{-1} with a maximum luminosity consistent with the Eddington limit for accreting X-ray sources. The current crop of transient sources appear to be more consistent with population II objects, and there may easily be a transient source somewhere in the galaxy every week. The typical lifetimes of these sources are shorter than the pre-1975 transient sources (the pulsating Centaurus and galactic center sources had lifetimes closer to a week than to several months), and the fact that they are preferentially found in richly populated regions of the plane makes them difficult to find with a source-confused experiment like this. Conversely, it is this same fact which favors their discovery by large field of view experiments which point for extended periods at just these regions. The relative paucity of UHURU transient sources may reflect a shorter average lifetime, as only a few, at most, would be "on" at any time.

Finally, with respect to what truly might be termed "fast transients", are some anomalous short-term increases we have observed. The first was reported by Holt, et al. (1974), and is displayed in Figure 14. The three matrices represent the same portion of the celestial sphere in three consecutive orbits, as the pointing direction did not change during this time. As indicated, an apparent "source" which was not present

in the first orbit appeared near the boundary between two elements in the second orbit, and was gone again in the third orbit. This "source" would have had an apparent luminosity of several photons $cm^{-2}sec^{-1}$ (i.e. in excess of the Crab Nebula) if it were present for the entire second orbit, but its absence from the first and third would indicate that its lifetime was probably shorter. The reality of the effect is solely dependent upon whether or not we can rule out all possible systematic aliasing, as we would have to wait $\sim 10^4$ years for a statistical variation like this.

If we consider the $\sim$ 60 most statistically significant candidate events of the type illustrated in Figure 14, more than half turn out to be clustered near the north and south auroral zones if we plot their celestial coordinates. We assume, therefore, that most (if not all) of these are geomagnetic in origin. It also means, however, that the remainder (including the event originally reported) have to be explained in some other way. Some of them are even repeating (i.e. within the same element or elements several orbits apart), but that does not reduce the possibility of a systematic error appreciably.

We have been unable to associate our remaining most-likely candidates with either gamma-ray bursts or flares in UHURU sources or UV Ceti stars. Our times are uncertain to the total integrated time of each orbit, but there are no IMP-7 gamma-ray burst candidates which are coincident. Similarly, the large error boxes in the positions we obtain do not always include any consistent class of associations. We are left, then, with an unverifiable phenomenon to report.

We cannot discount the strong possibility that the spacecraft data system is somehow responsible. Even though the double-counting of each photon guards against bit errors in the telemetry, we have no absolute assurance that the photons are properly recorded in the core store. The five most statistically significant events of this type (including that of Figure 14) were all recorded at the same spacecraft latitude as the sun. It is conceivable, therefore, that the dropping of a sector bit for a small amount of time can result in some solar counts being recorded as such an event. The a priori probability of all of the five most prominent events being at the solar lacitude is $\sim 10^{-5}$, so that the most conservative approach would be to assume that all of them are purely systematic. The prototype event, however, has two adjacent longitude elements contributing, so that the dropping of a single bit cannot (as in the case of a single element) "explain" the effect for this event. It still remains, therefore, our best example of an unexplained X-ray burst.

If any of them are real, the most likely candidates for association are flares in nearby stars (such as UV Ceti stars). The time scales are reminiscent of stellar flares, and the energy requirements are minimized the closer the phenomena are placed. We should not exclude the possibility of more exotic origins, like sudden increases in the accretion rates of otherwise quiescent binary systems with compact members resulting in a short-term increase to Eddington-limited luminosity. Rather than devoting our energy to explanations at this point in time, however, it is much more important that the effect first be verified. As there are no other

all-sky X-ray monitors in orbit, the only possibility for verification would seem to be accidental coincidences in optical coverage. Perhaps we will be lucky enough to find such coverage during an observation of one of these bursts, and perhaps (even luckier) the optical observation will be corroborative of a transient phenomenon.

Acknowledgments

The contributions of the many individuals which resulted in the successful launch and operation of Ariel-5 are noted, with thanks. In particular, the success of the All-Sky Monitor is the direct result of the efforts of the author's colleagues at the Goddard Space Flight Center: E. Boldt, U. Desai, L. Kaluzienski, E. Karageorge, and P. Serlemitsos.

References

Amnuel, P. R., Guseinov, O. H., and Rakhamimov, Sh. Ju. 1974 Astrophys. and Space Science 29, 331

Boldt, E. A., Holt, S. S., Rothschild, R. E., and Serlemitsos, P. J. 1975, in Proceedings of International Conference on X-Rays in Space, Calgary (D. Venkatesan, ed.) in press

Canizares, C. R., McClintock, J. E., Clark, G. W., Lewin, W. H. G., Schnopper, H. W., and Sprott, G. F. 1973, Nature Phys. Sci. 241, 28

Gottlieb, E. W., Wright, E. L., and Liller, W. 1975, Ap. J. (Letters) 195, L33

Holt, S. S., Kaluzienski, L. J., Boldt, E. A., and Serlemitsos, P. J. 1974, IAU Circular No. 2729

Hutchings, J. B., Crampton, D., Glaspey, J., and Walker, G. A. H. 1973, Ap. J. 182, 549

Li, F. K., and Clark, G. W. 1974, Ap. J. (Letters) 191, L27

Mason, K. O., Hawkins, F. J., Sanford, P. W., Murdin, P., and Savage, A. 1974, Ap. J. (Letters) 192, L65

Parsignault, D. R., Gursky, H., Kellogg, E. M., Matilsky, T., Murray, S., Schreier, E., Tananbaum, H., Giacconi, R., and Brinkman, A. C. 1972, Nature Phys. Sci. 239, 123

Pounds, K. 1974, IAU Circular No. 2729

Sanford, P. W., and Hawkins, F. H. 1972, Nature Phys. Sci. 239, 135

Silk, J. 1973, Ap. J. 181, 747

Tananbaum, H., Gursky, H., Kellogg, E., Giacconi, R., and Jones, C. 1972, Ap. J. (Letters) 177, L15

Figure Captions

(1) Isometric schematic of the experiment geometry. X-rays may enter only through one of the two pinholes, and are recorded on one of the two position-sensitive detectors mounted at 45° with respect to the spin axis. The instantaneous field of view of each detector is 4°x90°.

(2) Detector efficiency as a function of incident x-ray energy. A detector cross-section is also displayed, and the efficiency is only for the 1/6 of the counter volume which is used for x-ray analysis. The beryllium window has no supports which shadow any portion of this x-ray volume.

(3) 3-6 keV "efficiency" as a function of counter gain, for three representative spectra. The electronic thresholds are permanently set at 2.5 keV and 7.5 keV for nominal gain = 1.

(4) The disposition of the 512 all-sky resolution elements in spacecraft coordinates. The blacked-in regions are never acccessible to the experiment, while the lightly shaded elements are sometimes solar-contaminated (the sun may appear in either the upper or lower hemisphere, or neither if close to the spacecraft equator). The solar image shown of $\sim$ 4°x4° is a typical source image size.

(5) Single-orbit raw data from 5 strong sources, which were each confined (in this oribt) almost entirely to single resolution elements. Sco X-1 typically gives $\sim$ 300 counts, and the other sources $\sim$ 10-20. The background varies somewhat with spacecraft latitude, but is typically $\sim$ 2 counts per element.

(6) Cyg X-3 and Cyg X-1 single-orbit data taken through 17 March 1975 folded in 20 bins modulo .199681 d. Each orbit contributes to a single bin only, corresponding to the orbit mid-time. The χ^2 is for the hypothesis of a constant source intensity.

(7) Cyg X-1 and Crab Nebula ≤ half-day data taken through 17 March 1975 folded in 20 bins. The uppermost trace is Cyg X-1 data folded modulo 5.4d, the second modulo 5.60089 d, and the third modulo 5.3 d. The fourth trace is Crab Nebula data modulo 5.60089 d. The phase of all traces is such that 1974 275.259766 d is at the boundary of bins 10 and 11, and all χ^2 are for the hypothesis of a constant source intensity.

(8a) Daily Cyg X-1 average intensities up to the reorientation of the Ariel-5 spin axis to Cyg X-1 (when it passes out of the field of view of this experiment).

(8b) Half-day (or finer) resolution intensities for Cygnus X-1 during the early rise in the intensity of the source in April 1975.

(9) Sco X-1 single-orbit data taken through 17 March 1975 folded in 20 bins modulo 0.787313 d. The value of χ^2 is for the hypothesis of constant source intensity.

(10) Sco X-1 orbit-by-orbit history for a particularly disturbed period in January 1975. The overall average intensity for 3 months surrounding this observation is $16.5 cm^{-2} sec^{-1}$.

(11) Average values of Sco X-1 ratios of experimental to statistical variances as a function of accumulation time. The minimum accumulation time is one orbit.

(12) Light curve of transient source in Triangulum. For purposes of comparison, the Crab Nebula intensity is $1.4 cm^{-2} sec^{-1}$.

(13) Light curve for Triangulum compared with the synthetic nova light curve of Amnuel, et al. (1974), where phase = 0 is maximum luminosity and phase = 1 corresponds to a luminosity of one-tenth of maximum.

(14) Raw output for three consecutive orbits, the second of which contains an anomalously high "x-ray source" at the boundary between two resolution elements. The numbers outside the large boxes are grid-identifying coordinates for the data matrices displayed within the boxes.

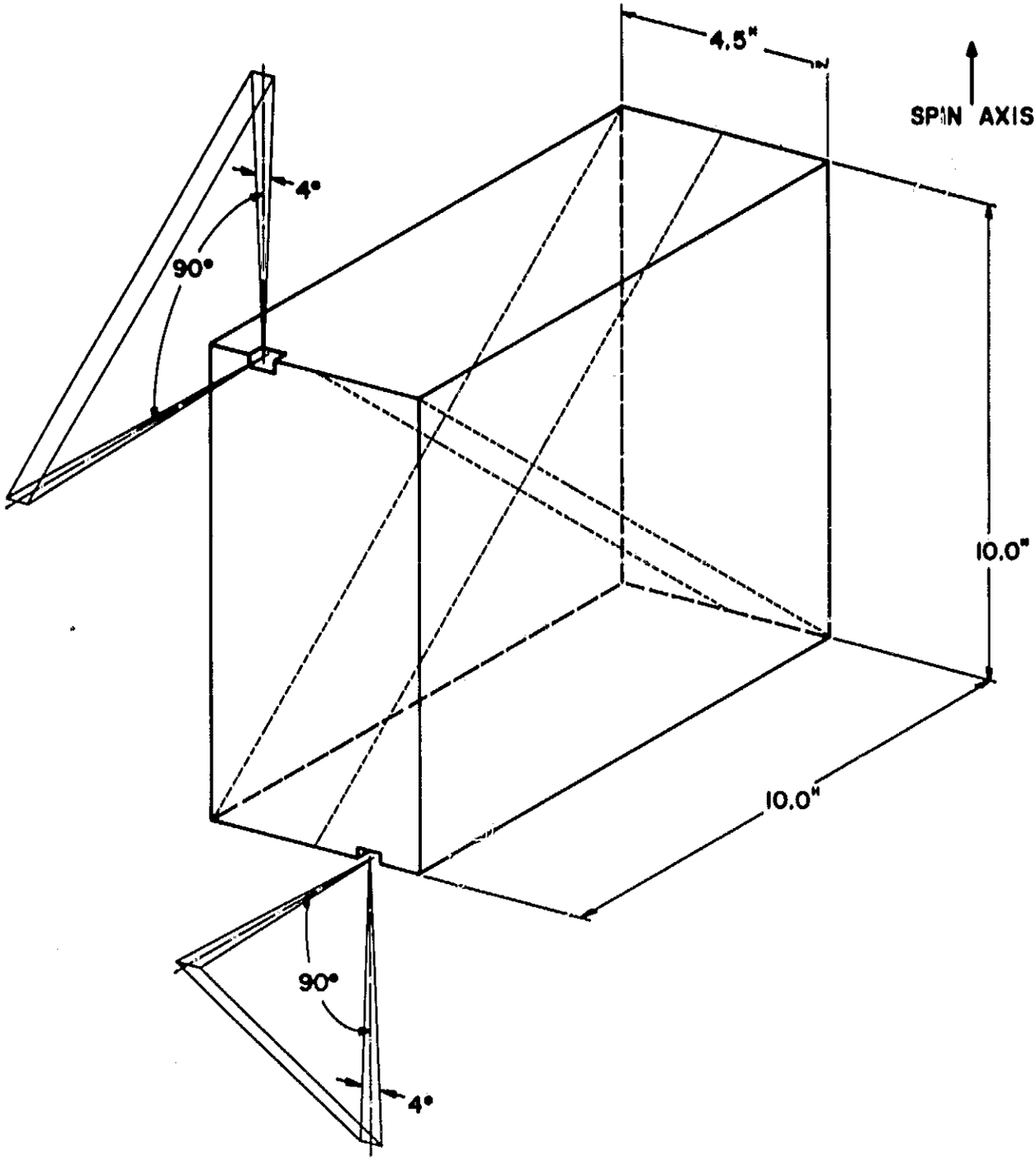

Fig. 1

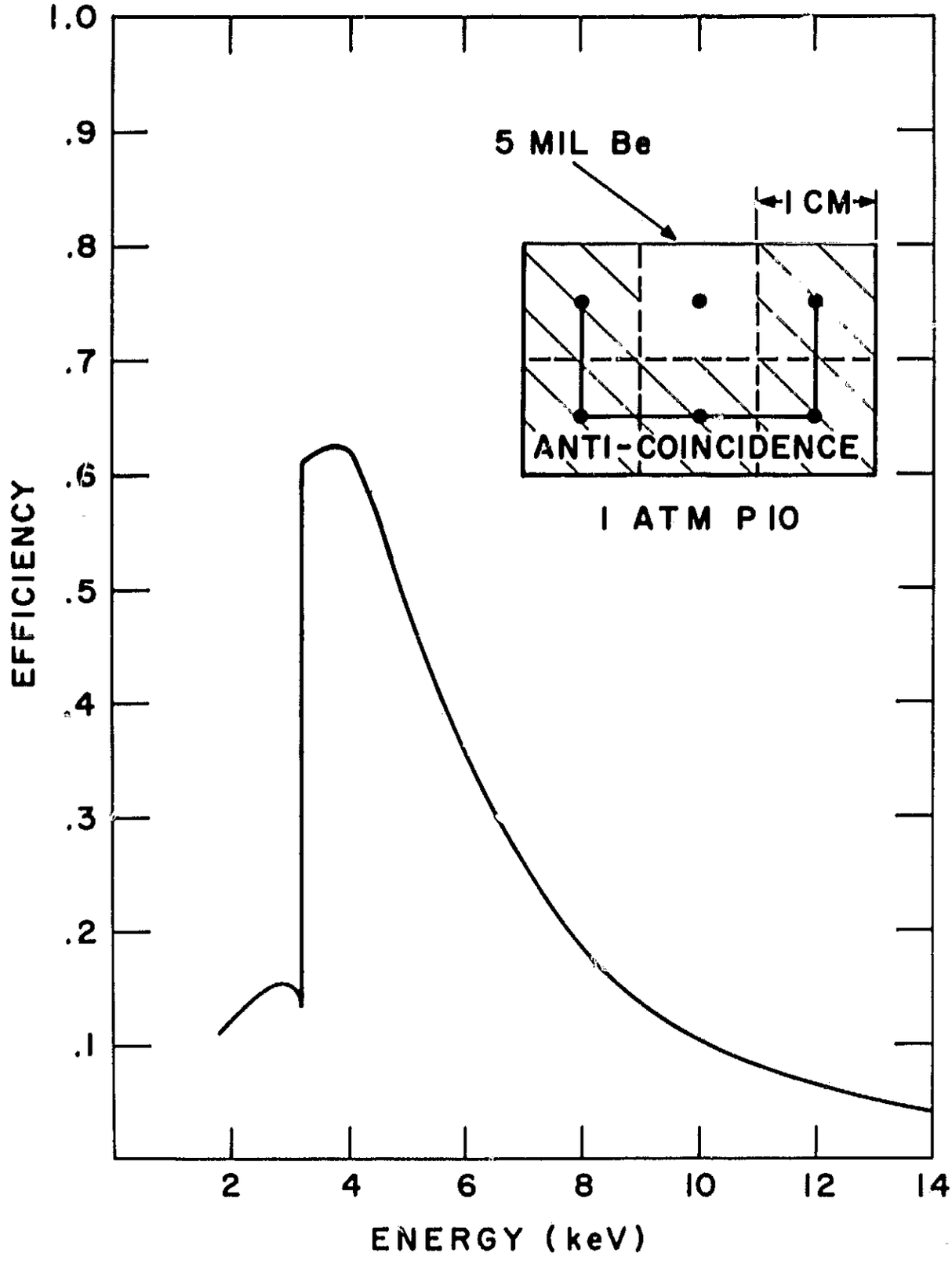
1.0
.9
.8
.7
.6
.5
.4
.3
.2
.1
EFFICIENCY
5 MIL Be
1 CM
ANTI-COINCIDENCE
1 ATM P10
2
4
6
8
10
12
14
ENERGY (keV)

Fig. 2

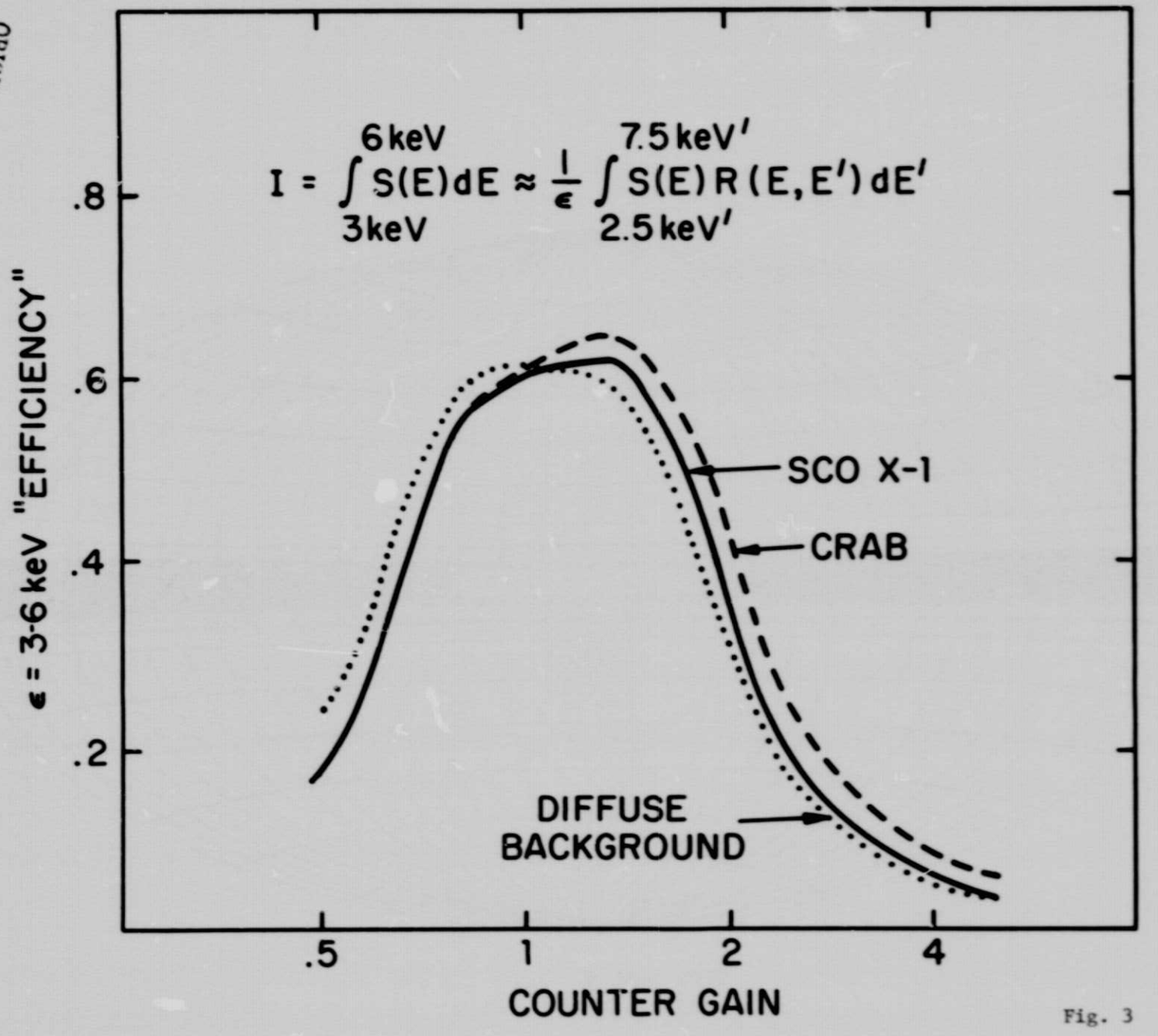

Fig. 3

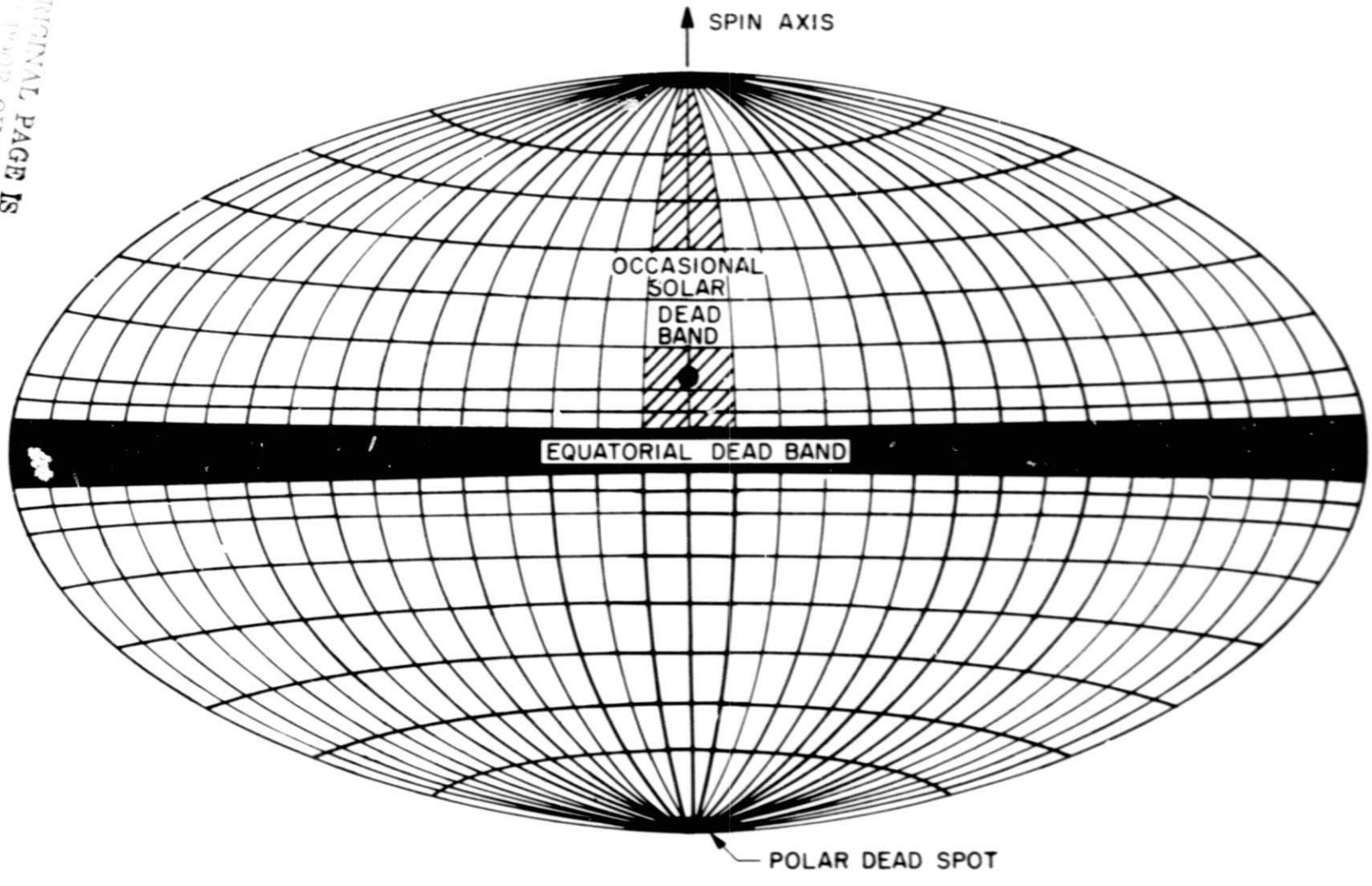

Fig. 4

"TYPICAL" CORE DUMP

MID-TIME 1975 6.0885d

ON-TIME 3552 sec

	6	3	4				
SCO X-1	2	287	4				
	2	1	1	4	3	5	7
				1	4	19	6
				3	4	6	7
				4	20	17	7
	2	2	3				
				0	6	5	5
CRAB	1	11	1				
	3	2	1				

CYG X-2

CYG X-1,3

Fig. 5

"TYPICAL" CORE DUMP

MID-TIME 1975 6.0885d

ON-TIME 3552 sec

6 3 4

SCO X-1 2 287 4

4 3 5 7

2 1 1

1 4 19 6 CYG X-2

3 4 6 7

4 20 17 7 CYG X-1,3

2 2 3

0 6 5 5

CRAB 1 11 1

3 2 1

Fig. 5

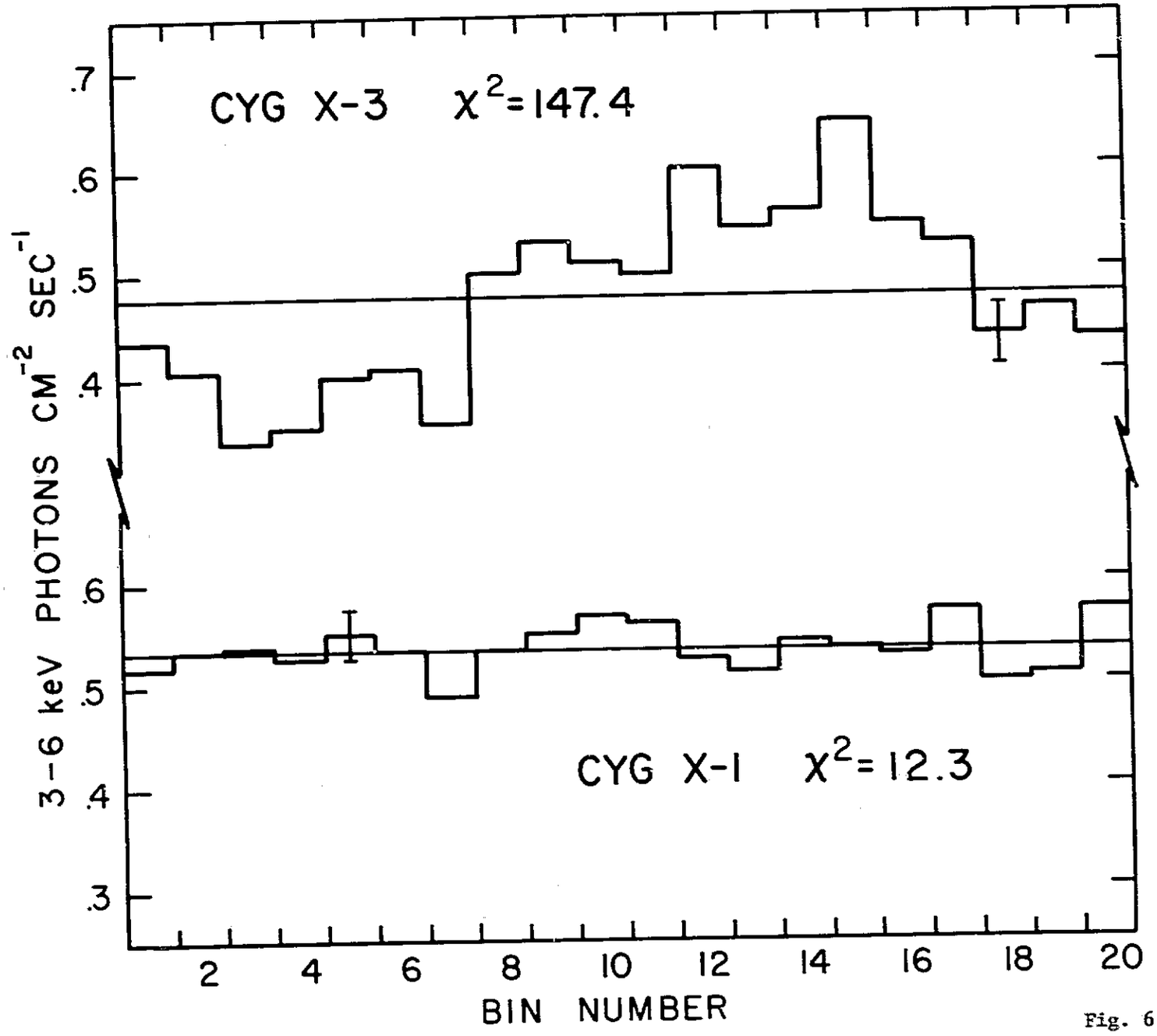
CYG X-3 χ^2=147.4
CYG X-1 χ^2=12.3
3-6 keV PHOTONS CM^{-2} SEC^{-1}
.7
.6
.5
.4
.6
.5
.4
.3
2
4
6
8
10
12
14
16
18
20
BIN NUMBER

Fig. 6

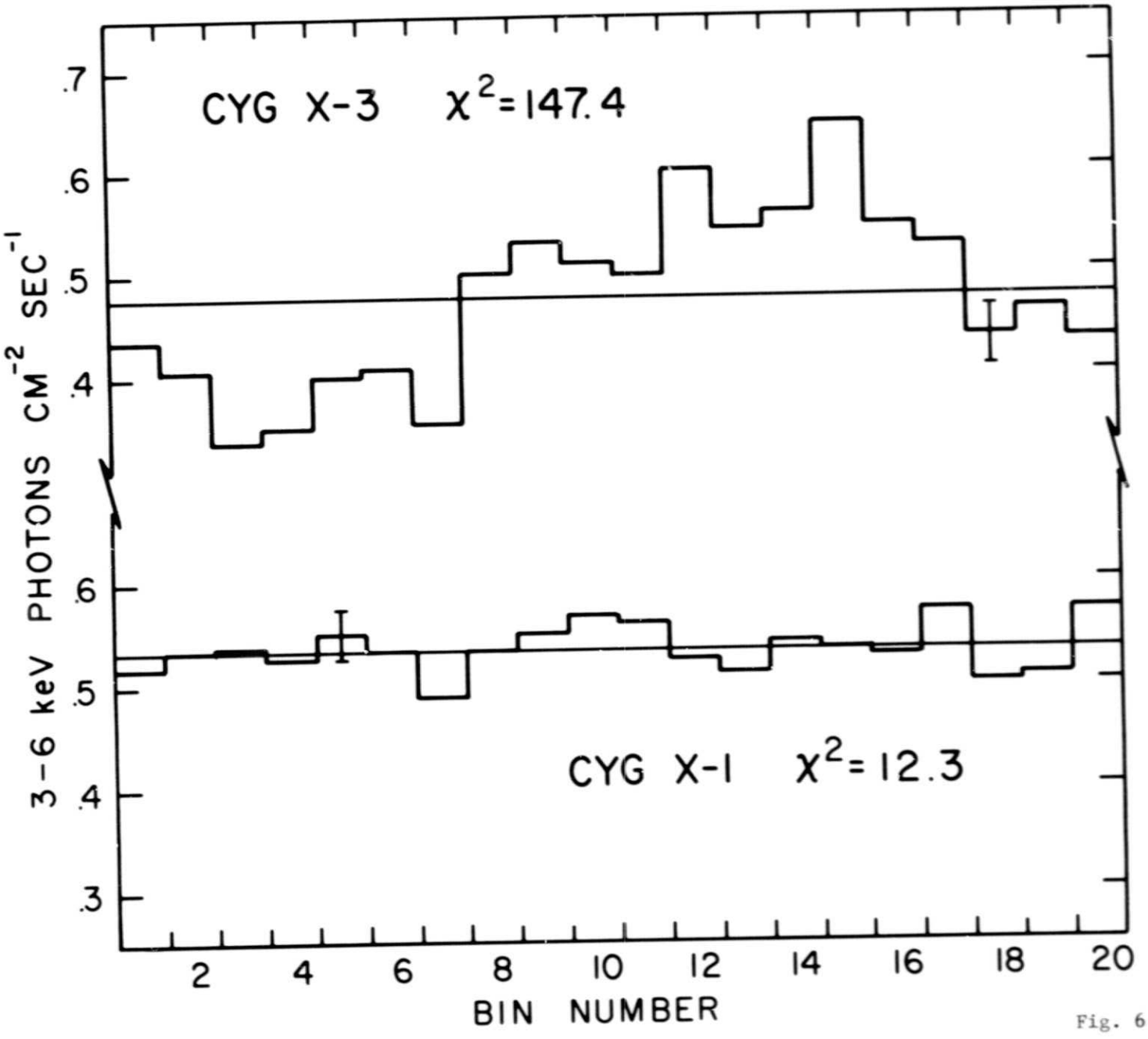
CYG X-3 X^2=147.4
CYG X-1 X^2=12.3
3-6 keV PHOTONS CM^{-2} SEC^{-1}
.7
.6
.5
.4
.6
.5
.4
.3
2
4
6
8
10
12
14
16
18
20
BIN NUMBER

Fig. 6

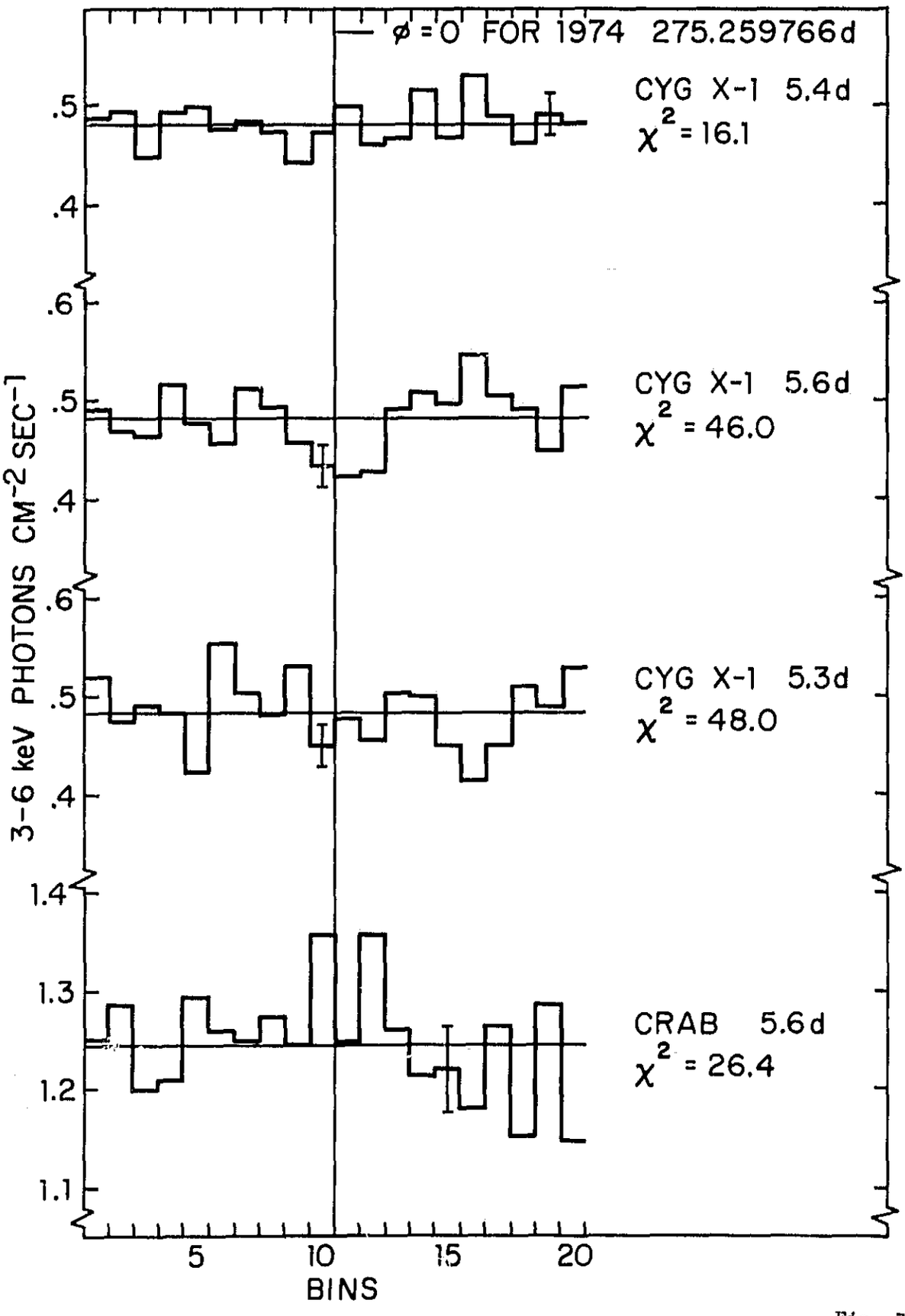
φ = 0 FOR 1974 275.259766d
CYG X-1 5.4d
χ² = 16.1
CYG X-1 5.6d
χ² = 46.0
CYG X-1 5.3d
χ² = 48.0
CRAB 5.6d
χ² = 26.4
3-6 keV PHOTONS CM⁻² SEC⁻¹
.5
.4
.6
.5
.4
.6
.5
.4
1.4
1.3
1.2
1.1
5
10
15
20
BINS

Fig. 7

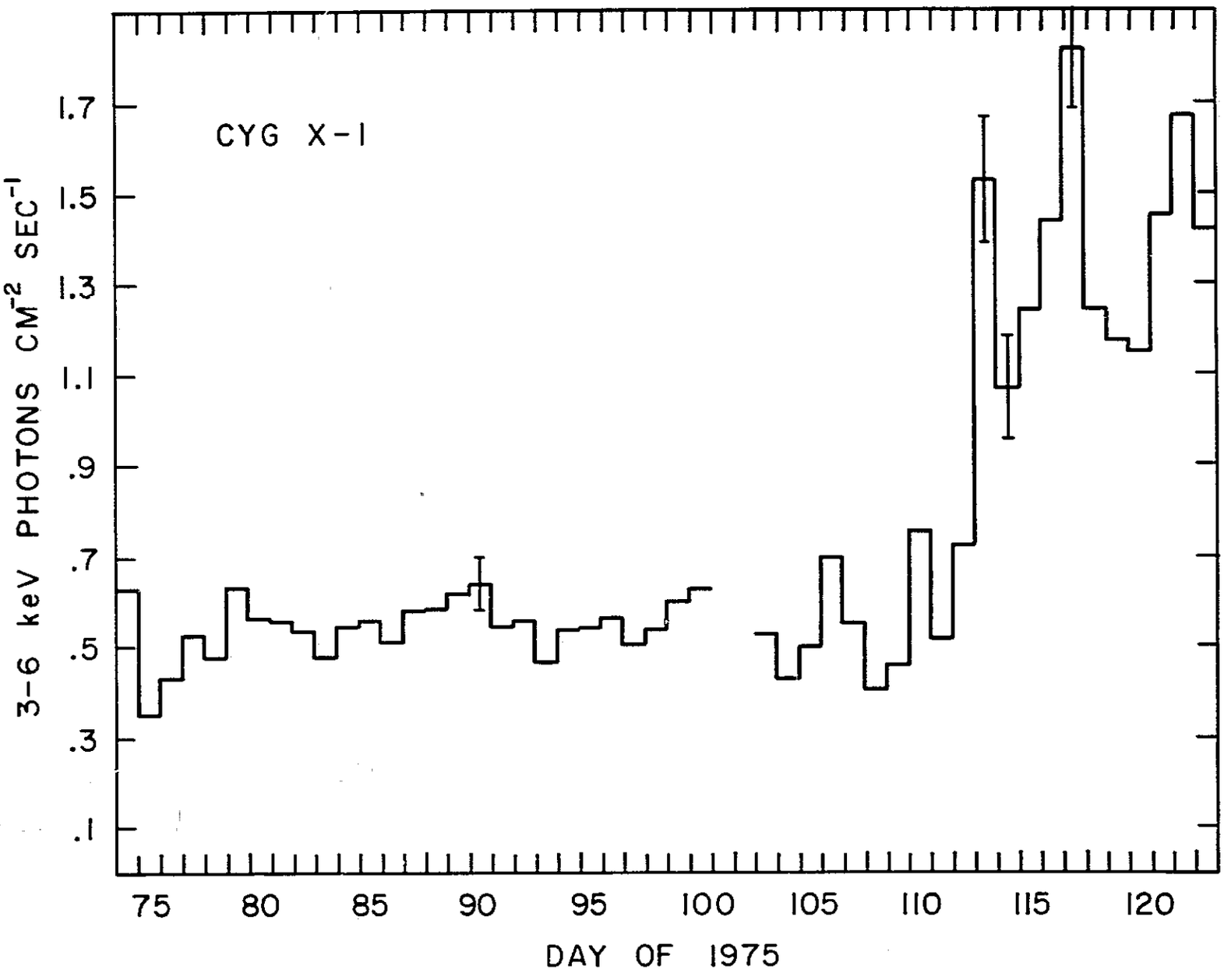

Fig. 8a

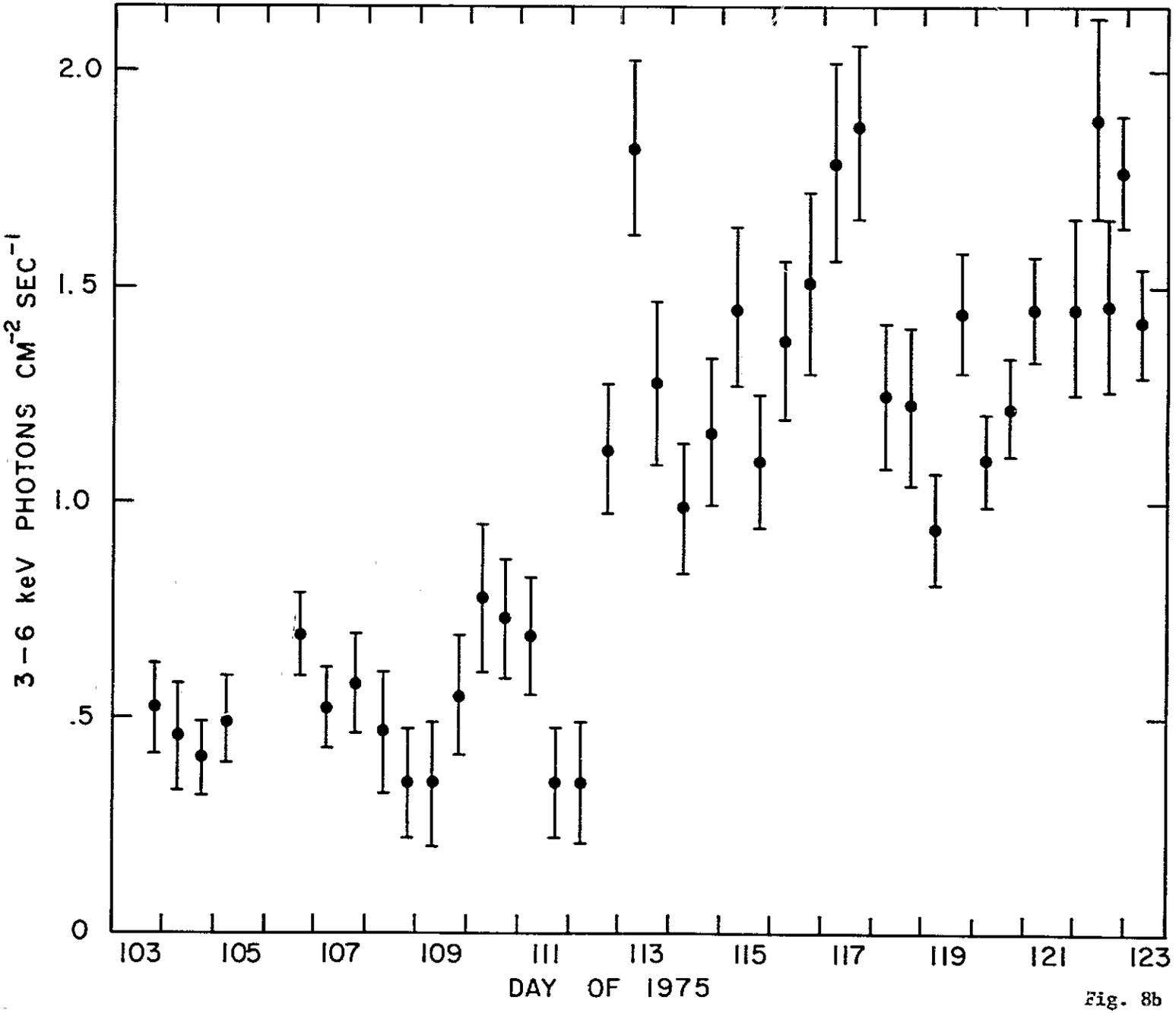
2.0
1.5
1.0
.5
0
3-6 keV PHOTONS CM^{-2} SEC^{-1}
103
105
107
109
111
113
115
117
119
121
123
DAY OF 1975

Fig. 8b

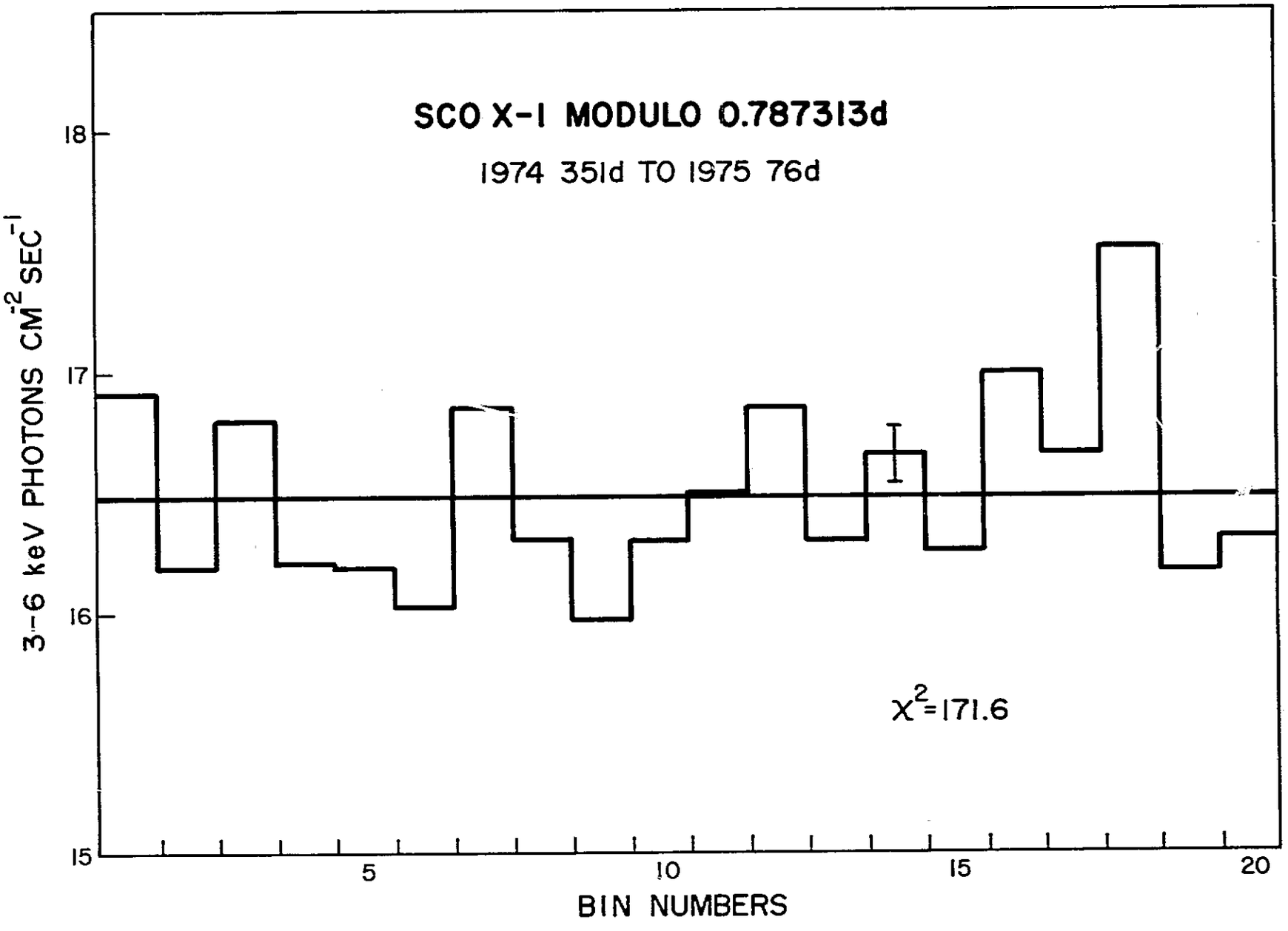
SCO X-1 MODULO 0.787313d
1974 351d TO 1975 76d
3-6 keV PHOTONS CM^{-2} SEC^{-1}
18
17
16
15
χ^2=171.6
5
10
15
20
BIN NUMBERS

Fig. 9

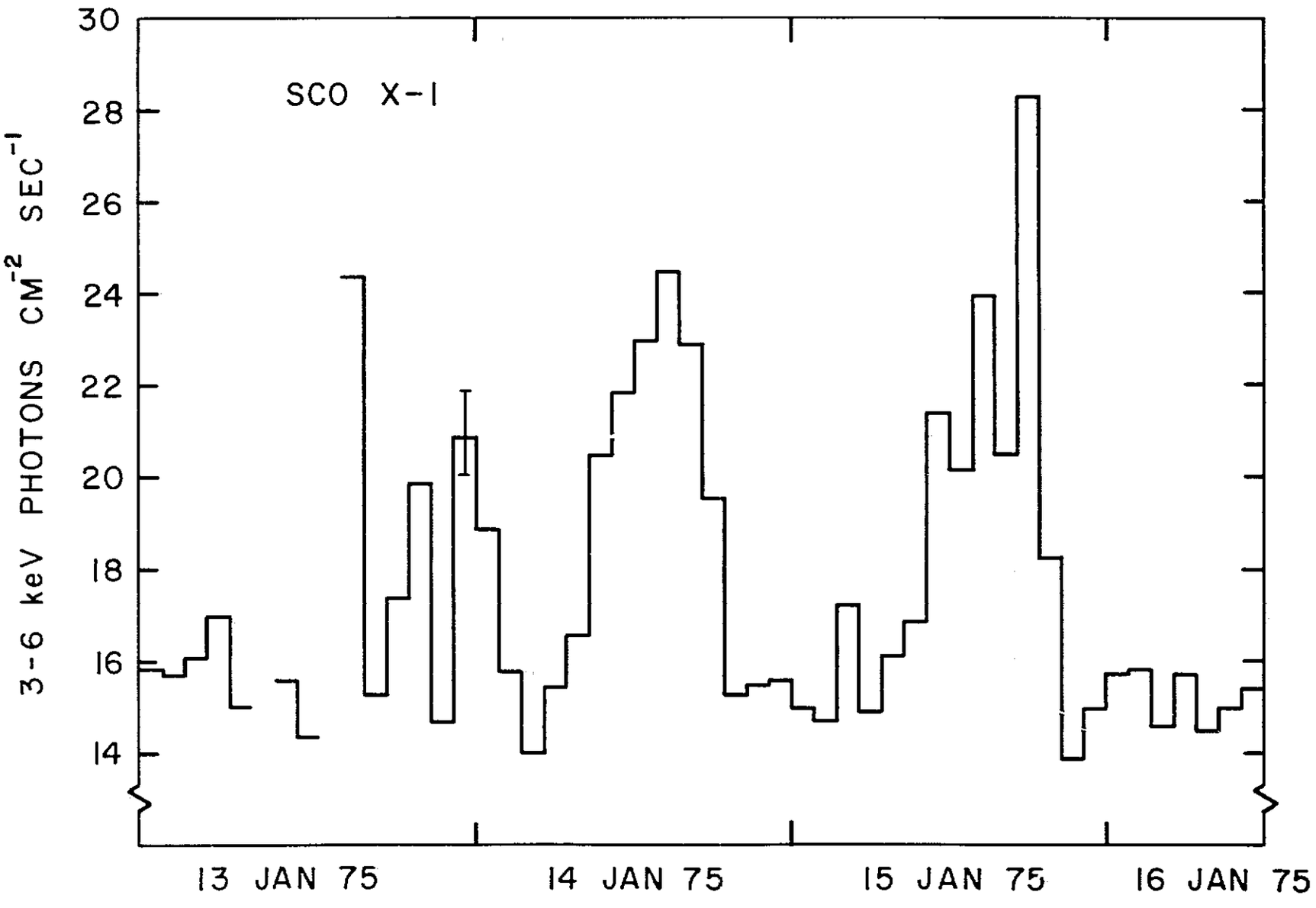
SCO X-1
3-6 keV PHOTONS CM^{-2} SEC^{-1}
30
28
26
24
22
20
18
16
14
13 JAN 75
14 JAN 75
15 JAN 75
16 JAN 75

Fig. 10

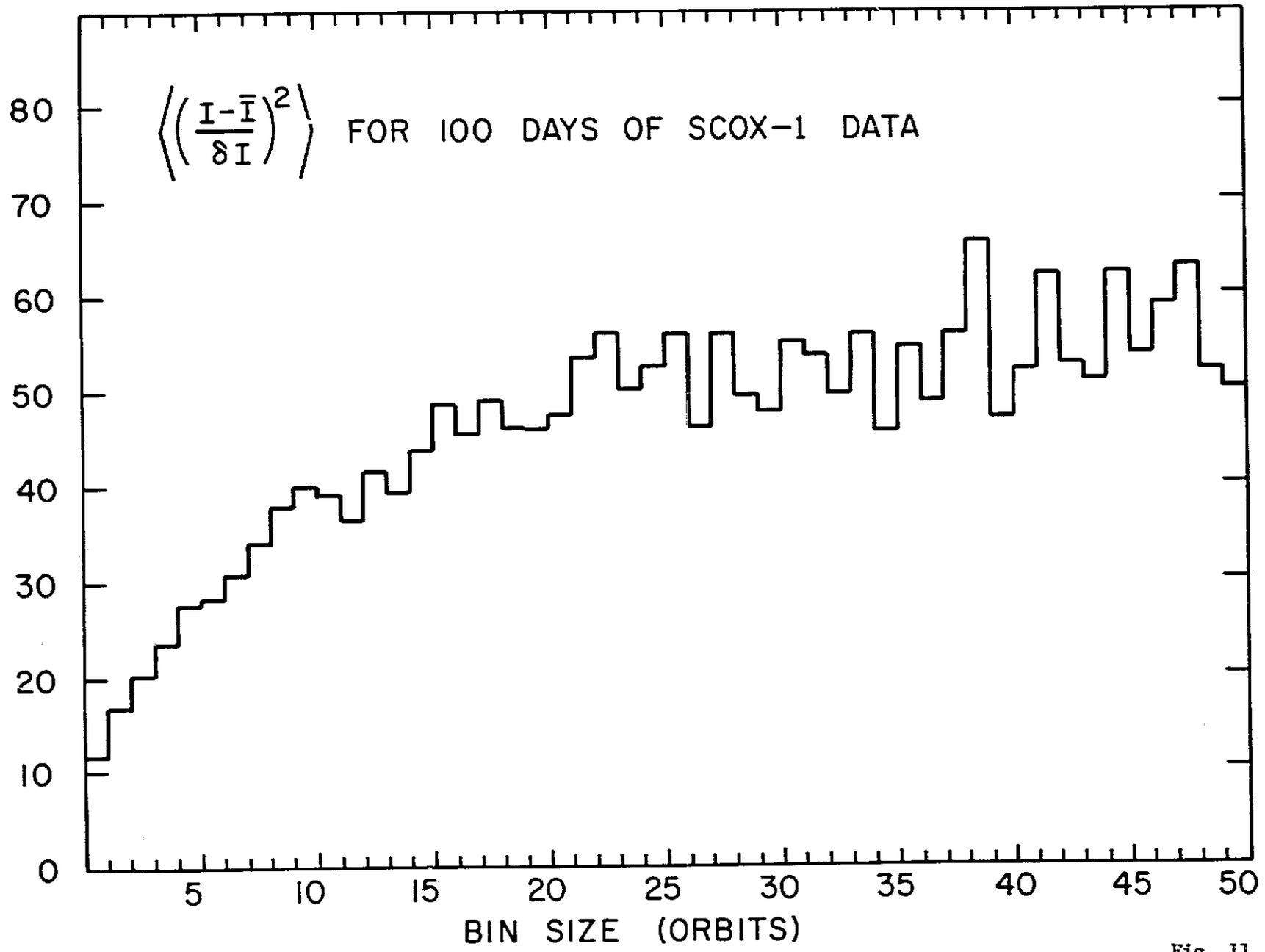
$\left\langle \left(\frac{I-\bar{I}}{\delta I} \right)^2 \right\rangle$ FOR 100 DAYS OF SCOX-1 DATA
80
70
60
50
40
30
20
10
0
5
10
15
20
25
30
35
40
45
50
BIN SIZE (ORBITS)

Fig. 11

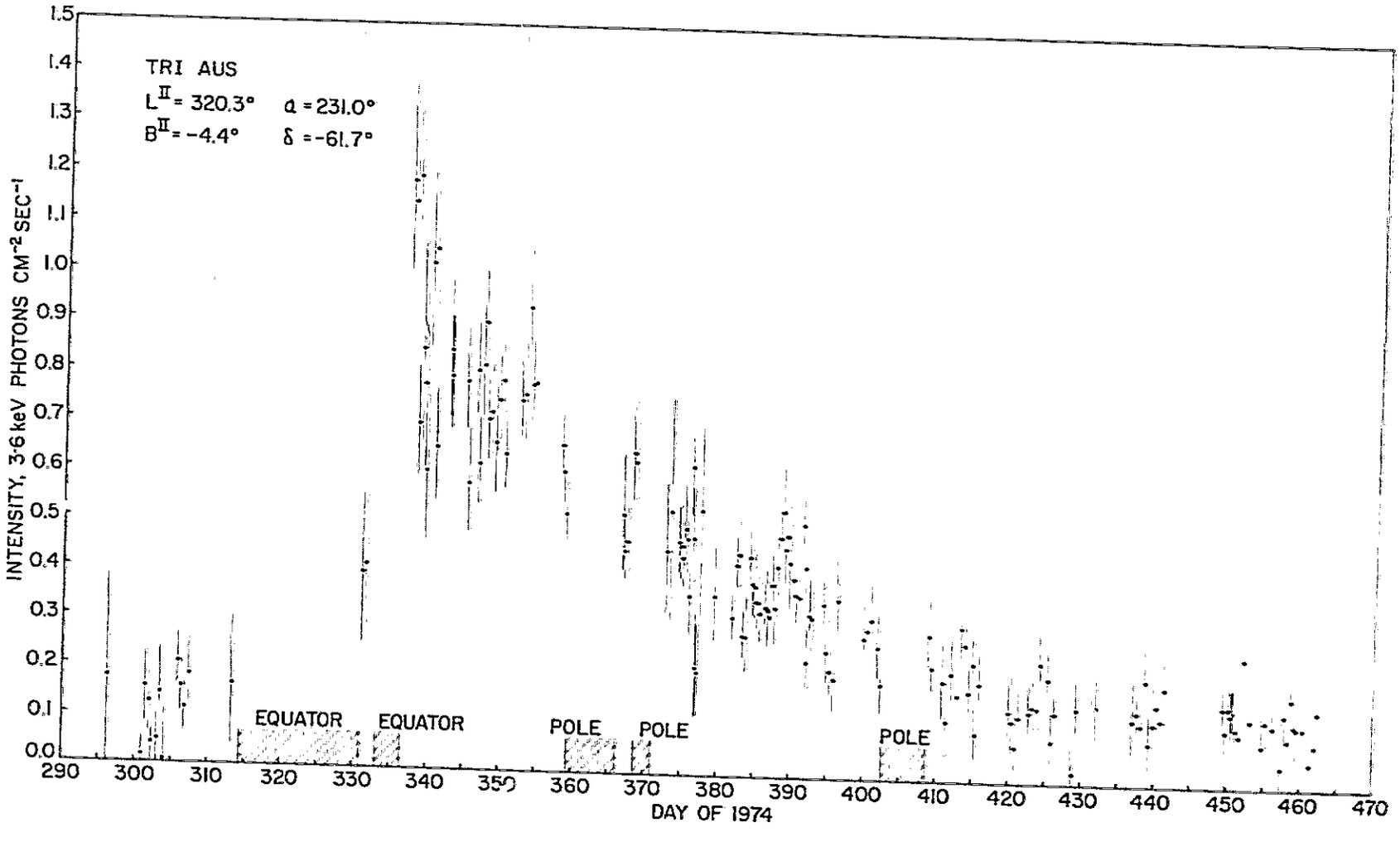
TRI AUS
L^{II} = 320.3° α = 231.0°
B^{II} = -4.4° δ = -61.7°
INTENSITY, 3-6 keV PHOTONS CM^{-2} SEC^{-1}
1.5
1.4
1.3
1.2
1.1
1.0
0.9
0.8
0.7
0.6
0.5
0.4
0.3
0.2
0.1
0.0
EQUATOR
EQUATOR
POLE
POLE
POLE
290
300
310
320
330
340
350
360
370
380
390
400
410
420
430
440
450
460
470
DAY OF 1974

Fig. 12

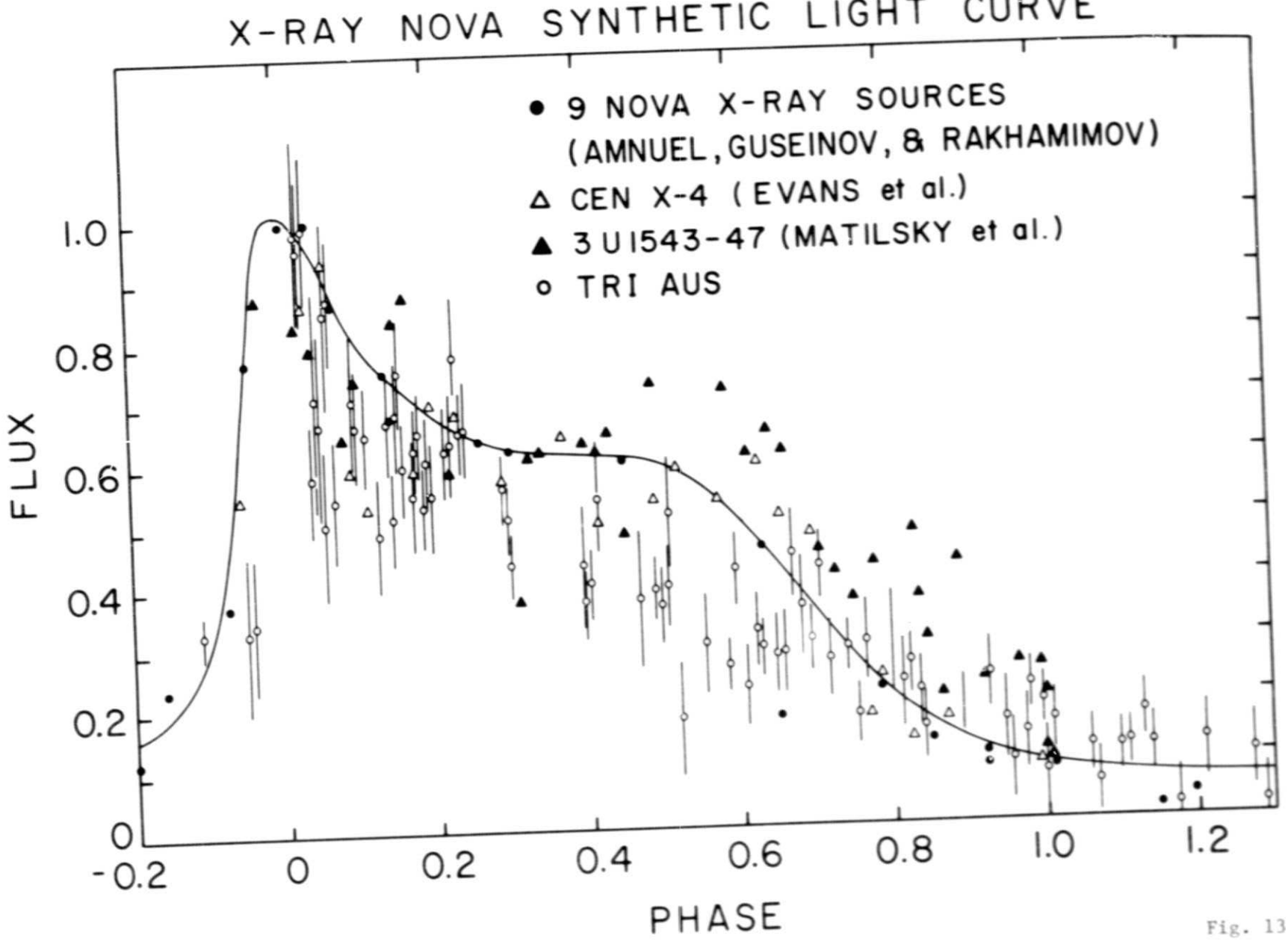
X-RAY NOVA SYNTHETIC LIGHT CURVE
• 9 NOVA X-RAY SOURCES
(AMNUEL, GUSEINOV, & RAKHAMIMOV)
△ CEN X-4 (EVANS et al.)
▲ 3U1543-47 (MATILSKY et al.)
o TRI AUS
FLUX
PHASE
0
0.2
0.4
0.6
0.8
1.0
-0.2
0
0.2
0.4
0.6
0.8
1.0
1.2

Fig. 13

	2	3	4	5	6	7
15	4	1	2	1	1	0
16	3	4	4	1	2	0
17	1	2	6	0	2	0
18	0	3	1	2	3	0
19	4	1	5	2	1	0
20	5	2	2	1	1	3

Orbit Number 532

1974 323 09 09 22

On-time: 3352 sec

15	3	4	1	5	2	2
16	5	1	4	3	0	2
17	1	2	3	15	3	0
18	1	4	5	20	1	2
19	2	4	2	4	2	0
20	1	4	4	3	1	0

Orbit Number 533

1974 323 10 50 22

On-time: 3456 sec

15	3	3	4	2	3	2
16	3	2	1	3	2	0
17	4	1	0	1	3	3
18	3	5	2	1	6	0
19	2	0	4	2	4	0
20	1	4	2	2	2	1

Orbit Number 534

1974 323 12 32 52

On-time: 3131 sec

Fig. 14